Reflection from Layered Surfaces due to Subsurface Scattering

Pat Hanrahan

Department of Computer Science
Princeton University

Wolfgang Krueger

Department of Scientific Visualization
German National Research Center
for Computer Science

Abstract

The reflection of light from most materials consists of two major terms: the specular and the diffuse. Specular reflection may be modeled from first principles by considering a rough surface consisting of perfect reflectors, or micro-facets. Diffuse reflection is generally considered to result from multiple scattering either from a rough surface or from within a layer near the surface. Accounting for diffuse reflection by Lambert's Cosine Law, as is universally done in computer graphics, is not a physical theory based on first principles.

This paper presents a model for subsurface scattering in layered surfaces in terms of one-dimensional linear transport theory. We derive explicit formulas for backscattering and transmission that can be directly incorporated in most rendering systems, and a general Monte Carlo method that is easily added to a ray tracer. This model is particularly appropriate for common layered materials appearing in nature, such as biological tissues (e.g. skin, leaves, etc.) or inorganic materials (e.g. snow, sand, paint, varnished or dusty surfaces). As an application of the model, we simulate the appearance of a face and a cluster of leaves from experimental data describing their layer properties.

CR Categories and Subject Descriptors: I.3.7 [Computer Graphics]: *Three-Dimensional Graphics and Realism*.

Additional Key Words and Phrases: Reflection models, integral equations, Monte Carlo.

1 Motivation

An important goal of image synthesis research is to develop a comprehensive shading model suitable for a wide range of materials. Recent research has concentrated on developing a model of specular reflection from rough surfaces from first principles. In particular, the micro-facet model first proposed by Bouguer in 1759 [4], and developed further by Beckmann[1], Torrance & Sparrow[26], and others, has been applied to computer graphics by Blinn [2] and Cook & Torrance[8]. A still more comprehensive version of the model was recently proposed by He et al[12]. These models have also been extended to handle anisotropic microfacets distributions[24, 5] and multiple scattering from complex microscale geometries[28].

Another important component of surface reflection is, however, diffuse reflection. Diffuse reflection in computer graphics has almost universally been modeled by Lambert's Cosine Law. This law states that the exiting radiance is isotropic, and proportional to the surface irradiance, which for a light ray impinging on the surface from a given direction depends on the cosine of the angle of incidence. Diffuse reflection is qualitatively explained as due to subsurface scattering [18]: Light enters the material, is absorbed and scattered, and eventually exits the material. In the process of this subsurface interaction, light at different wavelengths is differentially absorbed and scattered, and hence is filtered accounting for the color of the material. Moreover, in the limit as the light ray is scattered multiple times, it becomes isotropic, and hence the direction in which it leaves the material is essentially random. This qualitative explanation accounts for both the directional and colormetric properties of diffuse materials. This explanation is also motivated by an early proof that there cannot exist a micro-facet distribution that causes equal reflection in all outgoing directions independent of the incoming direction [10].

The above model of diffuse reflection is qualitative and not very satisfying because it does not refer to any physical parameter of the material. Furthermore, there is no freedom to adjust coefficients to account for subtle variations in reflection from different materials. However, it does contain the essential insight: an important component of reflection can arise from subsurface scattering. In this paper, we present a model of reflection of light due to subsurface scattering in layered materials suitable for computer graphics. The only other work in computer graphics to take this approach is due to Blinn, who in a very early paper presented a model for the reflection and transmission of light through thin clouds of particles in order to model the rings of Saturn[2]. Our model differs from Blinn's in that it is based on one-dimensional linear transport theory—a simplification of the general volume rendering equation [19]— and hence is considerably more general and powerful. Of course, Blinn was certainly aware of the transport theory approach, but chose to present his model in a simpler way based on probabilistic arguments.

In our model the relative contributions of surface and subsurface reflection are very sensitive to the Fresnel effect (which Blinn did not consider). This is particularly important in biological tissues which, because cells contain large quantities of water, are translucent. A further prediction of the theory is that the subsurface reflectance term is not necessarily isotropic, but varies in different directions. This arises because the subsurface scattering by particles is predominantly in the forward direction. In fact, it has long been known experimentally that very few materials are ideal diffuse reflectors (for a nice survey of experiments pertaining to this question, see [18]).

We formulate the model in the currently emerging standard terminology for describing illumination in computer graphics [16, 11]. We also discuss efficient methods for implementation within the context of standard rendering techniques. We also describe how to construct materials with multiple thin layers. Finally, we apply the model to two examples: skin and leaves. For these examples, we build on experimental data collected in the last few years, and provide pointers to the relevant literature.

Another goal of this paper is to point out the large amount of recent work in the applied physics community in the application of linear transport theory to modeling appearance.

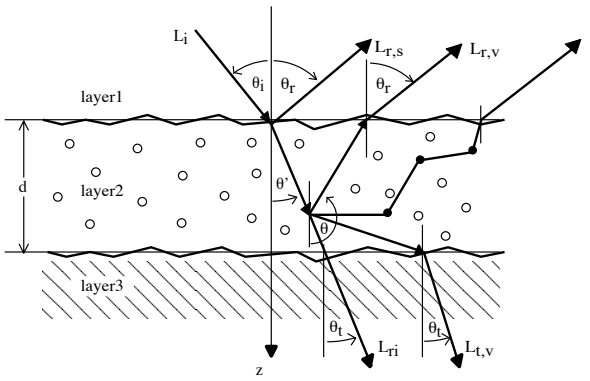

Figure 1: The geometry of scattering from a layered surface

(θ_i, ϕ_i)	Angles of incidence (incoming)
(θ_r, ϕ_r)	Angles of reflection (outgoing)
(θ_t, ϕ_t)	Angles of transmission
$L(z; \theta, \phi)$	Radiance [W / (m^2 sr)]
L_i	Incident (incoming) radiance
L_r	Reflected (outgoing) radiance
L_t	Transmitted radiance
L_+	forward-scattered radiance
L_-	backward-scattered radiance
$f_r(\theta_i, \phi_i; \theta_r, \phi_r)$	BRDF
$f_t(\theta_i, \phi_i; \theta_t, \phi_t)$	BTDF
$f_{r,s}(\theta_i, \phi_i; \theta_r, \phi_r)$	Surface or boundary BRDF
$f_{t,s}(\theta_i, \phi_i; \theta_t, \phi_t)$	Surface or boundary BTDF
$f_{r,v}(\theta_i, \phi_i; \theta_r, \phi_r)$	Volume or subsurface BRDF
$f_{t,v}(\theta_i, \phi_i; \theta_t, \phi_t)$	Volume or subsurface BTDF
n	Index of refraction
$\sigma_s(z; \lambda)$	Scattering cross section [mm^{-1}]
$\sigma_a(z; \lambda)$	Absorption cross section [mm^{-1}]
$\sigma_t(z; \lambda)$	Total cross section ($\sigma_t = \sigma_a + \sigma_s$) [$mm^{-1}$]
W	Albedo ($W = \frac{\sigma_s}{\sigma_t}$)
d	Layer thickness [mm]
$p(z; \theta, \phi; \theta', \phi'; \lambda)$	Scattering phase function ((θ', ϕ') to (θ, ϕ))

Table 1: Nomenclature

2 Reflection and Transmission due to Layered Surfaces

As a starting point we will assume that the reflected radiance L_r from a surface has two components. One component arises due to surface reflectance, the other component due to subsurface volume scattering. (The notation used in this paper is collected in Table 1 and shown diagramatically in Figure 1.)

$$L_r(\theta_r, \phi_r) = L_{r,s}(\theta_r, \phi_r) + L_{r,v}(\theta_r, \phi_r)$$

where:

$L_{r,s}$ - reflected radiance due to surface scattering

$L_{r,v}$ - reflected radiance due to volume or subsurface scattering

The models developed in this paper also predict the transmission through a layered surface. This is useful both for materials made of multiple layers, as well as the transmission through thin translucent surfaces when they are back illuminated. The transmitted radiance has two components. The first component is called the *reduced intensity*; this is the amount of incident light transmitted through the layer without scattering inside the layer, but accounting for absorption. The second is due to scattering in the volume.

$$L_t(\theta_t, \phi_t) = L_{ri}(\theta_t, \phi_t) + L_{t,v}(\theta_t, \phi_t)$$

where:

L_{ri} - reduced intensity

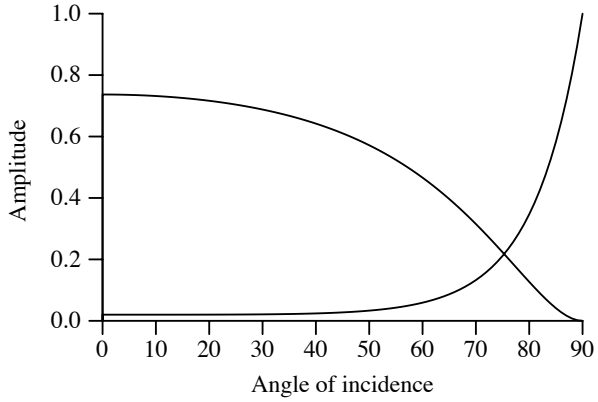

Figure 2: Fresnel transmission and reflection coefficients for a ray leaving air (n = 1.0) and entering water (n = 1.33).

$L_{t,v}$ - transmitted radiance due to volume or subsurface scattering

The bidirectional reflection-distribution function (BRDF) is defined to the differential reflected radiance in the outgoing direction per differential incident irradiance in the incoming direction [23].

$$f_r(\theta_i, \phi_i; \theta_r, \theta_r) \equiv \frac{L_r(\theta_r, \phi_r)}{L_i(\theta_i, \phi_i) \cos\theta_i d\omega_i}$$

The bidirectional transmission-distribution function (BTDF) has a similar definition:

$$f_t(\theta_i, \phi_i; \theta_t, \theta_t) \equiv \frac{L_t(\theta_t, \phi_t)}{L_i(\theta_i, \phi_i) \cos\theta_i d\omega_i}$$

Since we have separated the reflected and transmitted light into two components, the BRDF and BTDF also have two components.

$$\begin{aligned} f_r &= f_{r,s} + f_{r,v} \\ f_t &= f_{ri} + f_{t,v} \end{aligned}$$

If we assume a planar surface, then the radiance reflected from and transmitted across the plane is given by the classic Fresnel coefficients.

$$\begin{aligned} L_r(\theta_r, \phi_r) &= R^{12}(n_i, n_t; \theta_i, \phi_i \rightarrow \theta_r, \phi_r) L_i(\theta_i, \phi_i) \\ L_t(\theta_t, \phi_t) &= T^{12}(n_i, n_t; \theta_i, \phi_i \rightarrow \theta_t, \phi_t) L_i(\theta_i, \phi_i) \end{aligned}$$

where

$$\begin{aligned} R^{12}(n_i, n_t; \theta_i, \phi_i \rightarrow \theta_r, \phi_r) &= R(n_i, n_t, \cos\theta_i, \cos\theta_t) \\ T^{12}(n_i, n_t; \theta_i, \phi_i \rightarrow \theta_t, \phi_t) &= \frac{n_t^2}{n_i^2} T = \frac{n_t^2}{n_i^2}(1 - R) \end{aligned}$$

where R and T are the Fresnel reflection formulae and are described in the standard texts (e.g. Ishimura[14]) and θ_t is the angle of transmission. Besides returning the amount of reflection and transmission across the boundary, the functions R^{12} and T^{12}, as a side effect, compute the reflected and refracted angles from the Reflection Law ($\theta_r = \theta_i$) and Snell's Law ($n_i \sin\theta_i = n_t \sin\theta_t$). Note also the factor of $(n_t/n_i)^2$) in the transmitted coefficient of the above formula; this arises due to the change in differential solid angle under refraction and is discussed in Ishimura[pp. 154-155]. Plots of the Fresnel functions for the boundary between air and water are shown in Figure 2.

In our model of reflection, the relative contributions of the surface and subsurface terms are modulated by the Fresnel coefficients.

$$f_r = R f_{r,s} + T f_{r,v} = R f_{r,s} + (1 - R) f_{r,v}$$

Thus, an immediate prediction of the model is that reflection due to subsurface scattering is high when Fresnel reflection is low, since more light enters the surface layer. Notice in Figure 2 that the percentage of transmission is very high for a quite wide range of angles of incidence. Thus, the reflectance properties of materials impregnated with water or oil (dielectrics with low indices of refraction) are dominated by subsurface reflectance components at near perpendicular angles of incidence, and surface components at glancing angles of incidence.

Actually, light returning from the subsurface layers must refract across the boundary again. Thus, it will be attenuated by yet another Fresnel transmission factor. Recall that if light returns from a media with a higher index of refraction, then total internal reflection may occur. All light with an incident angle greater than the critical angle ($\theta_c = sin^{-1}\, n_i/n_t$) will not be transmitted across the boundary. By assuming an isotropic distribution of returning light, we can compute the percentage that will be transmitted and hence considered reflected. This sets an upper bound on the subsurface reflectance of $1 - (n_i/n_t)^2$ (remember, $n_t > n_i$). For example, for an air-water boundary, the maximum subsurface reflectance is approximately .44.

3 Description of Materials

The aim of this work is to simulate the appearance of natural materials such as human skin, plant leaves, snow, sand, paint, etc. The surface of these materials is comprised of one or more layers of material composed of a mixture of randomly distributed particles or inhomogeneities embedded in a translucent media. Particle distributions can also exist, in which case the properties are the material are given by the product of each particle's properties times the number of particles per unit volume.

The layers of such materials can be described by a set of macroscopic parameters as shown in the following table. Measurements of these properties have been made for a large variety of natural materials.

Symbol	Property
n	index of refraction
σ_a [mm^{-1}]	absorption cross section
σ_s [mm^{-1}]	scattering cross section
d [mm]	depth or thickness
$p(\cos j)$	scattering phase function
g	mean cosine of phase function

- *Index of Refraction*
  The materials considered are dielectrics where n is on the order of the index of refraction of water (1.33).
- *Absorption and scattering cross section*
  The intensity of the backscattered and transmitted light depends on the absorption and scattering properties of the material. The cross section may be interpreted as the probability per unit length of an interaction of a particular type. The total scattering cross section $\sigma_t = \sigma_a + \sigma_s$. The mean free path is equal to the reciprocal of the total cross section. An important quantity is the albedo, which equals $W = \sigma_s/\sigma_t$. If the albedo is close to 1, the scattering cross section is much greater than the absorption cross section, whereas if the albedo is close to 0, absorption is much more likely than scattering.
- *Scattering phase function*
  The phase function, $p(\vec{x}; \theta, \phi; \theta', \phi')$ represents the directional scattering from (θ', ϕ') to (θ, ϕ) of the light incident onto a particle. This function depends on the nature of the scattering medium. The form of p is affected by the size, form and orientation of the suspended particles, the dielectric properties of the particles, and the wavelength of the incident light. The scattering of light from particles small compared to the wavelength of light is given by the Rayleigh scattering formula, and the scattering due to dielectric spheres of different radii by the Mie formula.

  However, most materials contain distributions of particles of many different sizes, so simple single particle phase functions are not applicable. For this reason, we describe the material phase function with the empirical formula, the Henyey-Greenstein formula[13].

$$p_{HG}(\cos j) = \frac{1}{4\pi} \frac{1 - g^2}{(1 + g^2 - 2g\cos j)^{3/2}}$$

  where j is the angle between the incoming and the outgoing direction (if the phase function depends only on this angle the scattering is symmetric about the incident direction). The Henyey-Greenstein formula depends on a single parameter g, the mean cosine of the scattered light. The Henyey-Greenstein phase function for different values of g is shown in Figure 3. Note that if $g = 0$ the scattering is isotropic, whereas positive g indicates predominantly forward scattering and negative g indicates predominantly backward scattering.

Figure 3: Henyey-Greenstein phase function for $g = -.3$ and $g = .6$.

In the model employed in this paper, material properties are described macroscopically as averages over the underlying microscopic material property definitions. If the material is made of several components, the resulting properties of the composite materials can be computed by simple summation.

$$\sigma_a = \sum_{i=1}^{n} w_i\, \sigma_{a,i}$$

$$\sigma_s\, p(\cos j, g) = \sum_{i=1}^{n} w_i\, \sigma_{s,i}\, p(\cos j, g_i)$$

and so on. Here w_i is the volume fraction of the volume occupied by material i.

Another very important property of real materials is that the properties randomly vary or fluctuate. Such fluctuations cause variation in the appearance of natural surfaces. This type of fluctuation is easy to model with a random noise function or a texture map.

Optical propagation in random media has been studied in a variety of applications, including blood oximetry, skin photometry, plant physiology, remote sensing for canopies and snow, the paint and paper industry, and oceanic and atmospheric propagation. For many examples the macroscopic parameters have been measured across many frequency bands. A major attempt of our work is the simulation of the appearance of natural surfaces by using measured parameters to be inserted into the subsurface reflection and transmission formulas. This approach is similar to the attempt of Cook & Torrance [8] to simulate the appearance of metallic surfaces by using appropriate values for the refractive index and the roughness parameters.

4 Light Transport Equations

Linear transport theory is a heuristic description of the propagation of light in materials. Transport theory is an approximation to elec-

tromagnetic scattering theory, and hence cannot predict diffraction, interference or quantum effects. In particular, the specular reflection of light from rough surfaces whose height variation is comparable in size to the wavelength of incident light requires the full electromagnetic theory as is done in He et al[12]. A nice discussion of the derivation of transport theory from electromagnetism and the conditions under which it is valid is contained in an recent article by Fante[9]. The applicability of transport theory, however, has been verified by its application to a large class of practical problems involving turbid materials, including inorganic materials such as ponds, atmospheres, snow, sand and organic materials such as human skin and plant tissue[14].

Transport theory models the distribution of light in a volume by a linear integro-differential equation.

$$\frac{\partial L(\vec{x},\theta,\phi)}{\partial s} = -\sigma_t L(\vec{x},\theta,\phi) + \sigma_s \int p(\vec{x};\theta,\phi;\theta',\phi') L(\vec{x},\theta',\phi')\, d\theta'\, d\phi'$$

This equation is easily derived by accounting for energy balance within a differential volume element. It simply states that the change in radiance along a particular infinitesimal direction ds consists of two terms. The first term decreases the radiance due to absorption and scattering. The second term accounts for light scattered in the direction of ds from all other directions. Thus, it equals the integral over all incoming directions.

For layered media, the assumption is made that all quantities only depend on z and not on x and y. This assumption is valid if the incoming illumination is reasonably constant over the region of interest. It is also roughly equivalent to saying the reflected light emanates from the same point upon which it hits the surface. With this assumption, the above equation simplifies to

$$\cos\theta \frac{\partial L(\theta,\phi)}{\partial z} = -\sigma_t L(\theta,\phi) + \sigma_s \int p(z;\theta,\phi;\theta',\phi')\, L(\theta',\phi')\, d\theta'\, d\phi'$$

The above equation is an integro-differential equation. It can be converted to an equivalent double integral equation, whose solution is the same as the original integro-differential equation.

$$L(z;\theta,\phi) = \int_0^z e^{-\int_0^{z'} \sigma_t \frac{dz''}{\cos\theta}} \int \sigma_s(z')\, p(z';\theta,\phi;\theta',\phi')\, L(z';\theta',\phi')\, d\omega' \frac{dz'}{\cos\theta}$$

This is the basis of most current approaches to volume rendering.

The 1-dimensional linear transport equation must also satisfy certain boundary conditions. This is most easily seen by considering the forward and the backward radiance separately.

$$L(\theta,\phi) = L_+(\theta,\phi) + L_-(\pi-\theta,\phi)$$

Where L_+ is energy propagating in the positive z direction, and L_- in the negative direction. Note that L_- is defined to be a function of of $\pi-\theta$, the angle between the backward direction of propagation and the negative z axis. It is important to remember this convention when using formulas involving backward radiances.

At the top boundary the forward radiance is related to the incident radiance.

$$L_+(z=0;\theta',\phi') = \int f_{t,s}(\theta_i,\phi_i;\theta',\phi')\, L_i(\theta_i,\phi_i)\, d\omega_i$$

This simply states that the forward component of radiance entering the volume at the boundary is due to light transmitted across the surface. If we assume a planar surface and parallel incident rays, then $f_{t,s}$ equals the Fresnel transmission term times a δ-function that picks up the appropriate angle of incidence.

$$L_+(z=0;\theta',\phi') = T^{12}(n_i,n_t;\theta_i,\phi_i \to \theta',\phi') L_i(\theta_i,\phi_i)$$

In the more general case of a rough surface, $f_{t,s}$ is given by a transmission coefficient times the probability that light will refract in the desired direction.

The boundary conditions at the top let us formally state the contribution to reflection due to subsurface scattering in terms of the solution of the integral equation at the boundary $z=0$.

$$L_{r,v}(\theta_r,\phi_r) = \int f_{t,s}(\theta,\phi;\theta_r,\phi_r)\, L_-(z=0;\theta,\phi)\, d\omega$$

Assuming a planar surface, this integral simplifies to

$$L_{r,v}(\theta_r,\phi_r) = T^{21}(n_i,n_t;\theta,\phi \to \theta_r,\phi_r) L_-(z=0;\theta,\phi)$$

Similar reasoning allows the transmitted radiance to be determined from the boundary conditions at the bottom boundary.

$$L_{t,v}(\theta_t,\phi_t) = \int f_{t,s}(\theta,\phi;\theta_t,\phi_t)\, L_+(z=d;\theta,\phi)\, d\omega$$

Once again, assuming a smooth surface,

$$L_{t,v}(\theta_t,\phi_t) = T^{23}(n_2,n_3;\theta,\phi \to \theta_t,\phi_t) L_+(z=d;\theta,\phi)$$

Thus, the determination of the reflection functions has been reduced to the computation of $L_-(z=0)$ and $L_+(z=d)$—the solution of the one-dimensional transport equation.

5 Solving the Integral Equation

There are very few cases in which integro-differential equations can be directly solved. The most famous solution is for the case of isotropic scattering and was derived by Chandrasekhar[7, p. 124]. Even for this simple phase function the solution is anisotropic.

The classic way to solve such an equation is to write it in terms of the Neumann series. Physically, this can be interpreted as expanding the solution in terms of the radiance due to an integer number of scattering events. That is,

$$L = \sum_{i=0}^{\infty} L^{(i)}$$

where $L^{(0)}$ is the direct radiance assuming no scattering, $L^{(1)}$ is the radiance due to a single scattering event, and $L^{(i)}$ is the radiance due to i scattering events. Similar equations apply to the forward and backward radiances, $L_+^{(i)}$ and $L_-^{(i)}$.

The radiance due to the i scattering events can be written using the following recurrence.

$$L^{(i+1)}(z;\theta,\phi) = \int_0^z e^{-\int_0^{z'} \sigma_t \frac{dz''}{\cos\theta}} \int \sigma_s(z')\, p(z';\theta,\phi;\theta',\phi')\, L^{(i)}(z';\theta',\phi')\, d\omega' \frac{dz'}{\cos\theta}$$

This is the basis for most iterative approaches for numerically calculating transport quantities.

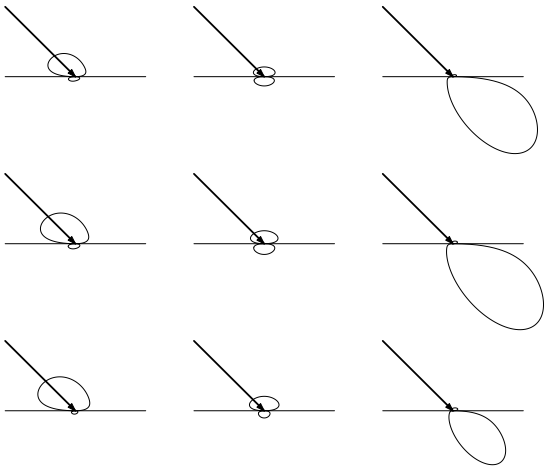

Figure 4: Solutions for $f_{r,v}^{(1)}$ and $f_{t,v}^{(1)}$ for different values of g and τ_d. From left to right the phase function shifts from predominately backward scattering ($g = -0.3$) to isotropic scattering ($g = 0.0$) to forward scattering ($g = 0.6$). From top to bottom the optical depth of the layer increases from 0.5 to 1.0 to 2.0.

5.1 First-Order Approximation

Another classic result in radiative transport, also derived by Chandrasekhar[7], is the analytic solution to the integral equation assuming only a single scattering event. As mentioned previously, this is equivalent to the method described by Blinn but derived using a completely different technique [2].

The 0th-order solution assumes that light is attenuated by the scattering and absorption, but not scattered. The attenuated incident light is called the *reduced intensity* and equals

$$L_+^{(0)}(z) = L_+(z=0)e^{-\tau/\cos\theta}$$

Here,

$$\tau(z) = \int_0^z \sigma_t \, dz$$

is called the *optical depth*. If σ_t is constant, then $\tau_d = \sigma_t d$.

Using the boundary conditions for incident and reflected light, and also rewriting the above equation in terms of the angles of incidence and reflection, we arrive at the following formula for the 0th-order transmitted intensity

$$L_{t,v}^{(0)}(\theta_t, \phi_t) = T^{12}T^{23}e^{-\tau_d}L_i(\theta_i, \phi_i)$$

By substituting the 0th-order solution, or reduced intensity, into the integral equation, the 1st-order solutions for forward and backward scattering can be calculated. The details of this calculation are described in Chandrasekhar and Ishimura and there is no need to repeat them here.

Using the boundary conditions for incident and reflected light, and also rewriting in terms of the angles of incidence and reflection, we arrive at the following formula for the backscattered radiance:

$$L_{r,v}^{(1)}(\theta_r, \phi_r) = WT^{12}T^{21}p(\pi-\theta_r, \phi_r; \theta_i, \phi_i)\frac{\cos\theta_i}{\cos\theta_i+\cos\theta_r}(1-e^{-\tau_d(1/\cos\theta_i+1/\cos\theta_r)})L_i(\theta_i, \phi_i)$$

This general formula shows that the backscattered light intensity depends on the Fresnel transmission coefficients, the albedo, the layer depth, and the backward part of the scattering phase function.

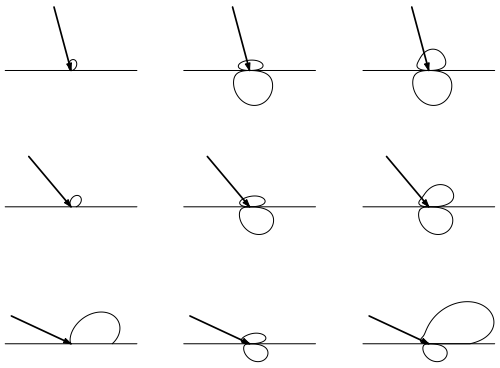

Figure 5: Solutions for f_r and f_t. In the left column is the surface specular reflection and in the middle is the subsurface reflection and transmission. On the right is the sum of surface and subsurface modulated by the Fresnel coefficients. From top to bottom the angle of incidence increases from 10 to 40 to 65 degrees.

A special case of this equation is Seeliger's Law, the first attempt to model diffuse reflection from first principles[25]. Seeliger's Law can be derived by assuming a semi-infinite layer ($\tau_d = \infty$) and ignoring Fresnel effects.

$$L_{r,v}(\theta_r, \phi_r) = \frac{\cos\theta_i}{\cos\theta_i + \cos\theta_r}L_i(\theta_i, \phi_i)$$

At the boundary $z = d$, the forward scattered radiance is given by

$$L_{t,v}^{(1)}(\theta_t, \phi_t) = WT^{12}T^{23}p(\theta_t, \phi_t; \theta_i, \phi_i)\frac{\cos\theta_i}{\cos\theta_i-\cos\theta_t}(e^{-\tau_d/\cos\theta_i}-e^{-\tau_d/\cos\theta_t})L_i(\theta_i, \phi_i)$$

For $\cos\theta_t = \cos\theta_i$, the singular factors can be avoided by using L'Hospital's rule, yielding

$$L_{t,v}^{(1)}(\theta_t, \phi_t) = WT^{12}T^{23}p(\theta_t, \phi_t; \theta_t, \phi_t)\frac{\tau_d}{\cos\theta_t}e^{-\tau_d/\cos\theta_t}L_i(\theta_t, \phi_t)$$

Figure 4 shows $f_{r,v}$ and $f_{t,v}$ for various values of g and d. Figure 5 shows the surface and subsurface components of the reflection model for various angles of incidence. These reflection and transmission distribution functions have several interesting properties:

1. The reflection steadily increases as the layer becomes thicker; in contrast, the transmission due to scattering increases to a point, then begins to decrease because of further scattering events.
2. Subsurface reflection and transmission can be predominately backward or forward depending on the phase function.
3. As the angle of incidence becomes more glancing, the surface scattering tends to dominate, causing both the reflection and the transmission due to subsurface scattering to decrease.
4. Due to the Fresnel effect, the reflection goes to zero at the horizons. Also, the reflection function appears "flattened" relative to a hemicircle. Thus, reflection for near normal angles of incidence varies less than Lambert's Law predicts.
5. The distributions vary as a function of reflection direction. Lambert's Law predicts a constant reflectance in all directions (which would be drawn as a hemicircle in these diagrams).

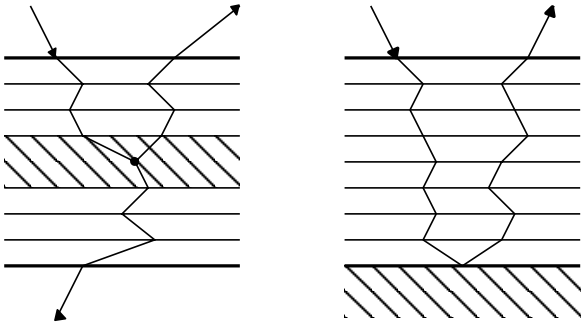

Figure 6: Determining first-order solutions for multiple layers. On the left, the contribution to the first order solution for a single layer. One the right, the contribution to the first order solution due to reflectance off a single layer.

The above formulas can be used to generate first-order solutions for multiple layers. (This is shown diagrammatically in Figure 6.) The total first-order scattering will be the sum of the first-order scattering from each layer, weighted by the percentage of light making it to the layer and returning from the layer. The percentage of light making it to the layer is the product of the 0th-order transmission functions (or reduced intensity) for a path through the layers above the reflecting layer. Similarly, the percentage of light leaving the entire layer after reflection is equal to the product of the 0th-order transmission functions for the path taken on the way out. Note that across each boundary the light may refract, and thus change direction and be attenuated by the Fresnel coefficient, but this is easy to handle. The process simplifies, of course, if each layer has the same index of refraction, since no reflection or change of direction occurs between layers. Given the above formulas it is very easy to construct a procedure to perform this calculation and we will make use of it in the results section.

The above formula can also be generalized to include reflection from a boundary between layers. In many situations reflection can only occur from the bottom layer. In this case, we add a single term accounting for the reduced intensity to reach the lower boundary, and also weight the returning light from that boundary. Such a model is commonly employed to model the reflection of light from a pool of water[15], and has been employed by Nishita and Nakamae[22]. Further generalizations of this type are described in Ishimura[14, p. 172].

6 Multiple Scattering

The above process of substituting the ith-order solution and then computing the integral to arrive at the (i+1)th-order solution can be repeated, but is very laborious. Note that subsequent integrals now involve angular distributions, because, although the input radiance is non-zero in only a single direction, the scattered radiance essentially comes from the directional properties of the phase function. Thus, this approach to solving the system analytically quickly becomes intractable.

We have implemented a Monte-Carlo algorithm for computing light transport in layered media. This algorithm is described in Figure 7. A thorough discussion of the application of Monte Carlo algorithms for layered media is discussed in the book [21], and the techniques we are using are quite standard.

To investigate the effects of multiple scattering terms, we simulated a semi-infinite turbid media with different albedos. The reflectance was computed and when the particles returning from the media are scored, we keep track of how many scattering events they underwent. Figure 8 shows the results of this experiment. The top curve is the total reflectance, and the lower curves represent scattering up to some order. Note that when the albedo is high, implying that $\sigma_s >> \sigma_a$, the first order term is only a small percentage of the total reflectance. However, as the albedo decreases, corresponding to greater absorption, a few low-order terms accurately approximate the reflectance. This effect can be explained by recalling that each term in the Neumann series representing the reflection is on the order of W^i, and since W is always less than one, the magnitude of higher-order terms quickly goes to zero.

1 *Initialize*: A particle enters the layer at the origin. Initialize $\vec{p}$ to the origin and the direction $\vec{s}$ to the direction at which the ray enters the layer. Set the weight $w = 1$.

2 *Events*: Repeat the following steps until the ray weight drops below some threshold or the ray exits the layer.

2A *Step*: First, estimate the distance to the next interaction:

$$d = -\frac{\log r}{\sigma_t}$$

Where r in this and the following formulas is a uniformly distributed random number between 0 and 1. Then, compute the new position:

$$\vec{p} = \vec{p} + d\,\vec{s}$$

And, finally set the particle weight to

$$w = w\frac{\sigma_s}{\sigma_s + \sigma_a}$$

Note: If d causes the particle to leave the layer, break from the repeat loop and adjust the weight using the distance to the boundary.

2B *Scatter*: First, estimate the cosine of the scattering angle for the Henyey-Greenstein phase function using the following formula.

$$\cos j = \frac{1}{|2g|}(1 + g^2 - (\frac{1 - g^2}{1 - g + 2gr})^2)$$

and $\cos\phi$ and $\sin\phi$ with $\phi = 2\pi r$. Then, compute the new direction:

$$\vec{t} = \begin{pmatrix} (\vec{s}.x\cos\phi\cos\theta - \vec{s}.y\sin\phi)/\sin\theta \\ (\vec{s}.y\cos\phi\cos\theta + \vec{s}.x\sin\phi)/\sin\theta \\ \sin\theta \end{pmatrix}$$

$$\vec{s} = \vec{s}\cos j + \vec{t}\sin j$$

Here, $\cos\theta = \vec{s}.z$ and $\sin\theta = \sqrt{1 - \vec{s}.z^2}$. Note: Care must be taken if $\sin\theta = 0$.

3 *Score*: Divide the sphere into regions of equal solid angle and add the weight of the particle to the weight associated with the bin in which it is contained.

Figure 7: Basic Monte Carlo algorithm for layered media

We have also computed the BRDF as a function of the angle of reflection using our Monte Carlo algorithm for the same configuration as described in the last experiment. The results are shown in Figure 9. Recall that the 1st-order reflection due to a semi-infinite media is given by Seeliger's Law: $\cos\theta_i/(\cos\theta_i + \cos\theta_r)$. The computed 1st-order BRDF matches the theoretical result quite well. In this figure we also plot the total BRDF due to any number of scattering events, and the difference between the total and the 1st-order BRDF. Note as in the previous experiment when the albedo W is small, the BRDF is closely approximated by the 1st-order term. However, note that the shape of the reflection function is also largely determined by the shape of the 1st-order reflection, which in turn is largely determined by the phase function. Fur-

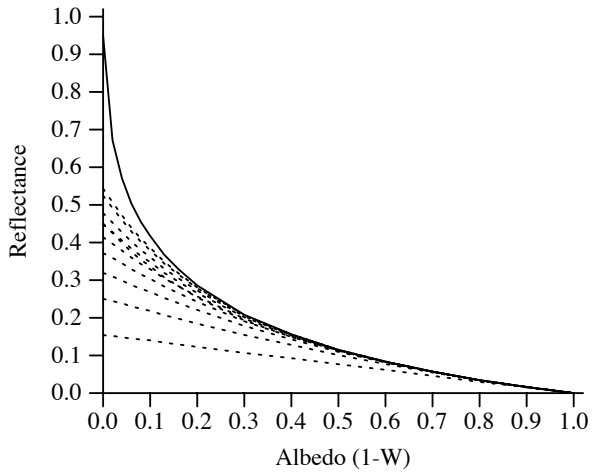

Figure 8: A plot of reflectance versus albedo for a semi-infinite media. The top curve is the total reflectance (the total radiant energy per unit area reflected divided by the incident irradiance). The bottom curve is the reflectance assuming only a single scattering event. Moving upward is a sequence of curves consisting of additional terms corresponding to a single additional scattering event. The first 10 terms in the solution are shown; In our simulations, we recorded terms involving thousands of scattering events.

ther, observe that the difference between the 1st-order solution and the full solution is approximately independent of the angle of reflection. Thus, the sum of the higher order terms roughly obeys Lambert's Law. For this reason it is often convenient to divide the subsurface reflection into two terms:

$$L_{r,v}(\theta_r, \phi_r) = L^{(1)}(\theta_r, \phi_r) + L^m$$

where L^m is constant and represents the sum of all the multiple scattering terms.

Finally, we have begun preliminary experiments where we incorporate a Monte Carlo subsurface ray tracer within a standard ray tracer. When the global ray tracer calls the subsurface ray tracer it attempts to estimate the BRDF and BTDF to a particular light source. This is done by *biasing* the Monte Carlo procedure to estimate the energy transported to the light. A simple method to do this is to send a ray to the light at each scattering event, as described in Carter and Cashwell[6]. This ray must be weighted by the phase function and the attenuation caused by the traversal through the media on the way to the light. If the albedo is less than 1, then only a few scattering events are important, and thus the subsurface ray tracer consumes very little time on average (the cost is proportional the the mean number of scattering events). Also, since the subsurface ray tracer does not consider the global environment when tracing its rays, the cost of subsurface Monte Carlo simulation at every shading calculation is relatively low. The advantage of this approach is that the BRDF's do not have to precomputed, and so if material parameters are varying across the surface, the correct answer is still estimated correctly at each point.

7 Results

The subsurface scattering models developed in this paper has been tested on two common natural surfaces: human skin and plant leaves. The goal of these experiments are twofold: First, to compare our anisotropic diffuse reflection model with Lambertian shading. Second, to attempt to simulate the optical appearance from measured parameters. Our experiments are meant to be suggestive of the power of this approach; we do not claim to have an experimentally validated model.

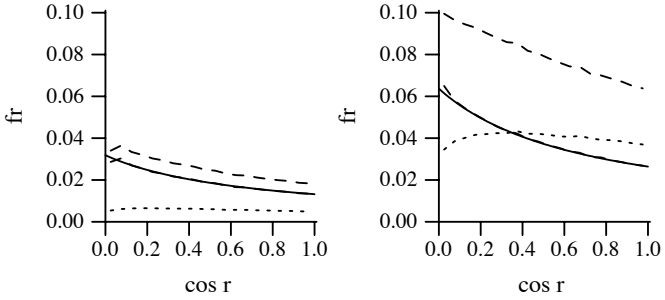

Figure 9: Graphs of the BRDF (f_r) as a function of the angle of reflection for a semi-infinite slab with different albedos (on the left $W = 0.4$ and on the right $W = 0.8$) and an angle of incidence of 45°. The solid line is the theoretical BRDF as given by Seeliger's Law (the superimposed dashed line is the computed 1st-order BRDF showing a good match). The top dashed curve is the total computed BRDF; The bottom dotted curve is the difference between the total BRDF due to multiple scattering events and the 1st-order BRDF.

Property	Epidermis	Dermis	Pigment	Blood
n	1.37-1.5	1.37-1.5	1.37-1.5	1.37-1.5
σ_a [mm^{-1}]	3.8	0.3		32.6
σ_s [mm^{-1}]	50.0	21.7		0.96
d [mm]	0.001-0.15	1-4		
g	0.79	0.81	.79	.0

Table 2: Two Layer Skin Model Properties. Pigment coefficients are mixed with epidermal coefficients to compute the properties of the outer layer. Blood coefficients are mixed with dermal coefficients to compute the properties of the inner layer.

7.1 Skin

Human skin can be modeled as two layers with almost homogeneous properties. Both layers are assumed to have the same refractive index but a different density of randomly distributed absorbers and scatterers. The outer epidermis essentially consists of randomly sized tissue particles and imbedded pigment particles containing melanin. The pigment particles act as strongly wavelength dependent absorbers causing a brown/black coloration as their density increases. The inner dermis is considered to be a composition of weakly absorbing and strongly scattering tissue material and of blood which scatters light isotropically and has strong absorption for the green and blue parts of the spectrum. Experimental evidence also supports the hypothesis that light scattering in the skin is anisotropic with significant forward scattering. A comprehensive study of optical properties of human skin can be found in van Gemert et al.[27]. The values chosen for our test pictures are given in Table 2. We also add a thin outer layer of oil that reflects light using the Torrance-Sparrow model of rough surfaces.

A head data set was acquired using a medical MRI scanner. Unfortunately, the ears and the chin were clipped in the process, but enough of the head is visible to test our shading models. A volume ray tracer was adapted to output the position and normal vector of the skin layer for each pixel into a file, and this input was used to evaluate the shading models described in this paper.

The influence of the various factors appearing in the subsurface reflection formula are shown on Plate 1. These pictures are

Plate 1.

Plate 2.

not shaded in the conventional way. In particular, a Lambertian shading model would yield a constant image. The first picture (upper left) shows the influence of the Fresnel factors. Observe that the intensity is almost flat, but strongly attenuated for glancing incident and viewing angles. The second picture (upper middle) shows the action of Seeliger's Law alone. Seeliger's Law leads to very little variation in shading, which makes the surface appear even more chalky or dusty. The third picture (upper right) demonstrates the action of the factor accounting for the finite layer depth giving only weak enhancements for glancing angles. This is a minor effect. The fourth picture (lower left) shows the influence of the Henyey-Greenstein scattering phase function for small backward scattering ($g = -.25$) and the fifth picture (lower middle) shows the effect of large forward scattering ($g = .75$). The result is strong enhancement of glancing reflection for low angles of incidence and viewing, assuming they are properly aligned. The last picture (lower right) shows the superposition of these four factors with $g = .75$ giving a complex behavior. An overall smoothing of the reflection appears; the surface appears to be more "silk-like" (see also Plate 3). Although these effects are all subtle, their combination when controlled properly can create a wide variation in appearance.

The appearance of the face with the new subsurface reflection model is compared to the Lambertian diffuse reflection model for different angles of incidence in Plate 2. The left column shows the results for the Lambert scattering for angles 0 and 45 degrees, and the middle column is rendered for the new model. Again, notice a much smoother "silk-like" appearance. The right column gives the relative difference of both models, red indicates more reflection from the new model, and blue vice versa.

Plate 3: Dark complexion controlled by setting the concentration of melanin. On the left are images with just subsurface scattering. On the right, an specular surface term is added to simulate an oily coat. In these pictures $g = .65$.

Plate 4: Human face with variation in subsurface blood concentration, an oily outer layer and Gaussian variation in parameters to create the "freckles."

To illustrate the degrees of freedom of the model, we rendered several faces with their parameters controlled by texture maps. One texture map controls the relative concentration of blood in the dermis; another texture map controls the concentration of melanin in the epidermal layer. These faces are shown in Plates 3 and 4. To create a dark complexion we modulate the percentage of pigment in the otherwise transparent epidermis. This creates a dark brown appearance due to the strong absorption of melanin (in this case we set the absorption to .6). For the lips the epidermis is set to be very thin such that the appearance is dominated by the reflection from the dermis which has for the lips a large blood content (strong absorption for green and blue light component). The epidermis pigment part also has been varied locally with about 20% with a Gaussian process. This allows us to create a wide variety of skin colors, from black to suntanned to Caucasian, and from flushed to burnt to relaxed. The pictures in Plate 3 also show the effect of an additional specular term due to a thin layer of oil on the skin. Finally, Plate 4 shows another picture created by our program.

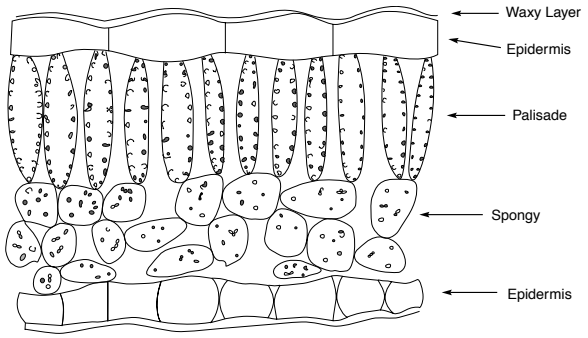

Figure 10: Typical leaf cross-section (Redrawn from [20]).

Plate 5: Leaf Model. On the left is the albedo image and on the right is a thickness image (white indicates thick)

This picture took approximately 20 seconds to render on a Silicon Graphics Personal Iris.

7.2 Leaves

Figure 10 shows an idealized leaf in cross-section. The leaf is composed of several layers of cells. On the top and bottom are epidermal cells with a thin smooth, waxy cuticular outer layer. The waxy cuticular layer is largely responsible for specularly reflected light. Below the upper epidermal cells there are a series of long palisaide cells which are highly absorbing due to the numerous chloroplasts contained within them. Below the palisaide cells are a loosely packed layer of irregularly shaped spongy cells. The spaces between the spongy cells are filled with air, which causes them to scatter light. Both the palisaide and the spongy cells are quite large (approximately 20 μm) compared to the wavelength, so their scattering phase function is forward directed. Furthermore, the cells are high in water content, so the index of refraction of the leaf is approximately equal to that of water—1.33. A typical leaf is .5 to 1 mm thick, with an optical depth of 5 to 10.

To test our model on a leaf, we constructed a leaf model using the technique described in Bloomenthal[3]. Although spectral transmission and reflectance curves are available for leaves[29], we have set the color of the leaf from an image acquired from a digital scanner. An albedo image is texture mapped onto a series of simply-shaped, bent polygons to create the leaf. Where the texture map is transparent the polygon is considered transparent and the leaf is not visible. We also modulate the thickness of the leaf with a thickness map drawn on top of the original leaf image. The texture maps we used are shown in Plate 5. The waxy cuticle is modeled using a rough specular surface with a specular exponent of 10. The interior of the leaf is modeled as a single homogeneous layer with an optical depth of 5 and a mean scattering cosine of .3[20].

Pictures were generated by modifying a conventional ray tracer to account for subsurface reflection and transmission. When a ray encounters a leaf, the BRDF and BTDF are evaluated for direct illumination from light sources. Shadow rays are cast to the light source, and if the ray stabs any other leaves the light intensity is attenuated by the 0th-order transmission function through each leaf. Plate 6 shows a picture of a cluster of leaves with the sun in different positions. Note that the reflection from leaves is largely determined by specular reflection due to the waxy cuticle; there is very little diffuse reflection and hence when the light source is on the same side of the leaf as the viewer, the leaf is quite dark. The transmission term, however, can be quite large, and therefore the leaves may actually be brighter when the are illuminated from behind. Note also that the increased thickness of the veins cause dark shadows to be cast on other leaves. The veins also appear dark when the leaf is back lit because they absorb more light, and bright when the leaf is front lit because their increased thickness causes more light to be reflected.

Plate 6: A cluster of leaves. A series of leaf images under different simulated lighting conditions. On the left are two backlit images, on the right, front lit.

8 Summary and Discussion

We have presented a reflectance model consisting of two terms: the standard surface reflectance and a new subsurface reflectance due to backscattering in a layered turbid media. This model is applicable to biological and inorganic materials with low indices of refraction, because their translucent nature implies that a high percentage of the incident light enters the material, and so the subsurface reflection is quite large. This model incorporates directional scattering within the layer, so the resulting subsurface reflection is not isotropic. This model can be interpreted as a theoretical model of diffuse reflectance. Thus, this model predicts a directionally varying diffuse reflection, in contrast to Lambert's Law. However, if multiple scattering contributes significantly to the reflection, then the higher scattering terms contribute to a reflection function with roughly the same shape.

As in any model, our model makes many assumptions. The two most important are that the physical optics may be approximated with transport theory, and that the material can be abstracted into layered, turbid media with macroscopic scattering and absorption properties. An "exact" model of biological tissues would explicitly model individual cells, organelles and so on, in considerably more detail. The Monte-Carlo algorithm for simulating reflection by Westin et al.[28] is an example of such an approach. Although such an approach may seem more accurate, often the experimental data needed to describe the arrangements of these structures is simply not available, and so in the end the results may be difficult to validate. An advantage of the transport theory approach is that the parameters of the model often may be directly extracted from experimental data.

A legitimate criticism of our work is that we did not directly compare the predictions of our model with experiment. The predictions of our model and the influence of measured material parameters should be checked carefully. However, we believe that this model has many applications in computer graphics even if it does not perfectly predict measured reflection functions. The metaphor of layered surfaces is very easy for users to understand because is a natural way to describe phenomenologically the appearance of many materials. It also fits easily into most rendering systems and can be implemented efficiently.

Finally, transport theory is a heuristic theory based on abstracting microscopic parameters into statistical averages. Transport theory is also the basis of the rendering equation, which is widely viewed as the correct theoretical framework for global illumination calculations. In this paper we propose to model surface reflection from layered surfaces with transport theory. Thus, when our reflectance model for layered surfaces is incorporated into a ray tracer, there is a hierarchy of transport calculations being performed. Within this hierarchy, the lower level transport equation computes the reflectance for the higher level transport equation. When performing this calculation, the lower level transport equation uses as its initial conditions the values from the higher level transport solution. Thus the two levels are coupled in a very simple way. In fact, it is possible to reformulate transport theory entirely in terms of reflection functions, the result is an integral equation for the reflection function itself; in this formulation the radiance does not appear at all. Coupling transport equations at different levels of detail in this manner is a promising approach to tackling the problem of constructing representations with many different levels of detail as proposed by Kajiya[17].

9 Acknowledgements

We would like to thank Craig Kolb for his help with RayShade and the leaf pictures. We would also like to thank David Laur for his help with the color plates. This research was partially supported by Apple, Silicon Graphics Computer Systems, David Sarnoff Research Center, and the National Science Foundation (CCR 9207966).

References

[1] BECKMANN, P., AND SPIZZICHINO, A. *The scattering of electromagnetic waves from rough surfaces*. Pergamon, Oxford, 1963.

[2] BLINN, J. F. Light Reflection Functions for Simulation of Clouds and Dusty Surfaces. *Computer Graphics 16*, 3 (July 1982), 21–29.

[3] BLOOMENTHAL, J. Modeling the Mighty Maple. *Computer Graphics 19*, 3 (July 1985), 305–311.

[4] BOUGUER, P. *The Gradation of Light*. University of Toronto Press, 1960.

[5] CABRAL, B., MAX, N., AND SPRINGMEYER, R. Bidirectional reflection functions from surface bump maps. *Computer Graphics 21*, 4 (July 1990), 273–281.

[6] CARTER, L., AND CASHWELL, E. *Particle Transport Simulation with the Monte Carlo Method*. Energy Research and Development Administration, 1975.

[7] CHANDRASEKHAR, S. *Radiative Transfer*. Dover, New York, 1960.

[8] COOK, R. L., AND TORRANCE, K. E. A Reflection Model for Computer Graphics. *ACM Transactions on Graphics 1*, 1 (1982), 7–24.

[9] FANTE, R. Relationship between Radiative Transport Theory and Maxwell's Equations in Dielectric Media. *J. Opt. Soc. Am. 71*, 4 (April 1981), 460–468.

[10] GRAWBOSKI, L. *Astrophysics J. 39* (1914), 299.

[11] HANRAHAN, P. From Radiometry to the Rendering Equation. *SIGGRAPH Course Notes: An Introduction to Radiosity* (1992).

[12] HE, X. D., TORRANCE, K. E., SILLION, F. X., AND GREENBERG, D. P. A Comprehensive Physical Model for Light Reflection. *Computer Graphics 25*, 4 (July 1991), 175–186.

[13] HENYEY, L. G., AND GREENSTEIN, J. L. Diffuse radiation in the galaxy. *Astrophysics J. 93* (1941), 70–83.

[14] ISHIMURA, A. *Wave Propagation and Scattering in Random Media*. Academic Press, New York, 1978.

[15] JERLOV, N. G. *Optical Oceanography*. Elsevier, Amsterdam, 1968.

[16] KAJIYA, J. Radiometry and Photometry for Computer Graphics. *SIGGRAPH Course Notes: State of the Art in Image Synthesis* (1990).

[17] KAJIYA, J. Anisotropic Reflection Models. *Computer Graphics 19*, 3 (July 1985), 15–22.

[18] KORTUM, G. *Reflectance Spectroscopy*. Springer-Verlag, Berlin, 1969.

[19] KRUEGER, W. The Application of Transport Theory to the Visualization of 3-D Scalar Fields. *Computers in Physics 5* (April 1991), 397–406.

[20] MA, Q., ISHIMURA, A., PHU, P., AND KUGA, Y. Transmission, Reflection and Depolarization of an Optical Wave For a Single Leaf. *IEEE Transactions on Geoscience and Remote Sensing 28*, 5 (September 1990), 865–872.

[21] MARCHUK, G., MIKHAILOV, G., NAZARALIEV, M., DARBINJAN, R., KARGIN, B., AND ELEPOV, B. *The Monte Carlo Methods in Atmospheric Optics*. Springer Verlag, Berlin, 1980.

[22] NAKAMAE, E., KANEDA, K., OKAMOTO, T., AND NISHITA, T. A Lighting Model Aiming at Drive Simulators. *Computer Graphics 24*, 4 (August 1990), 395–404.

[23] NICODEMUS, F. E., RICHMOND, J. C., AND HSIA, J. J. *Geometrical Considerations and Reflectance*. National Bureau of Standards, October 1977.

[24] POULIN, P., AND FOURNIER, A. A Model for Anisotropic Reflection. *Computer Graphics 24*, 4 (August 1990), 273–282.

[25] SEELIGER, R. *Munch. Akad. II. Kl. Sitzungsber 18* (1888), 201.

[26] TORRANCE, K. E., AND SPARROW, E. M. Theory of Off-Specular Reflection From Roughened Surfaces. *Journal of the Optical Society of America 57* (September 1967), 1104–1114.

[27] VAN GEMERT, M. F. C., JACQUES, S. L., STERENBERG, H. J. C. M., AND STAR, W. M. Skin Optics. *IEEE Transactions on Biomedical Engineering 36*, 12 (December, 1989), 1146–1154.

[28] WESTIN, S. H., ARVO, J. R., AND TORRANCE, K. E. Predicting Reflectance Functions from Complex Surfaces. *Computer Graphics 26*, 2 (July 1992), 255–264.

[29] WOOLLEY, J. T. Reflectance and Transmittance of Light by Leaves. *Plant Physiology 47* (1971), 656–662.